Streamlined Tuning Procedure for Stable PID Control of Flexible-Base Manipulators

Marc-André Bégin, Ryan Poon, and Ian Hunter, *Life Member, IEEE*

***Abstract*—The successful control of robotic manipulators mounted on flexible bases such as suspended mobile robots requires more sophisticated controllers than those employed for fixed-based manipulators. Solutions proposed in the literature often require expert knowledge to tune control parameters or lack stability guarantees when the dynamics of the flexible base lie close to those of the manipulator in the frequency domain. This letter addresses these issues by introducing a tuning procedure for the linear PID gains of a manipulator mounted on a flexible base that guarantees stability. A publicly available Python library implementing this procedure is also introduced to streamline the process for a wide array of user-defined models. The performance of a controller generated using this procedure is shown in simulations for a 3DOF manipulator mounted on an 8-legged tracked vehicle.**

***Index Terms*—Field robots, motion control, underactuated robots.**

I. Background

MOBILE manipulators mounted on passively suspended vehicles constitute a special class of underactuated robots. These flexible-base actuators are notoriously harder to control than their fixed-base counterparts due to the coupling between the dynamics of the vehicle and the manipulator. Some illustrative robotics examples include robots designed for crop scouting (Fig. 1), intervening on search-and-rescue missions, or interacting with the environment during interplanetary exploration.

In some of the earliest work on the topic, Hootsman and Dubowsky derived an expression for a hybrid Mobile Manipulator Jacobian (MMJ) that relates the generalized velocities of the end-effector to those of the vehicle and manipulator joints [1], [2]. The authors then demonstrated that classic control approaches for fixed-base manipulators can be adapted using this MMJ to successfully control the end-effector position of a mobile manipulator. For fast motion, Torres observed that the base of the manipulator is still likely to oscillate after the end-effector first reaches its target pose [3]. To help dampen these vibrations, the authors proposed to switch the joint-space PD gains of the controller to maximize energy transfer from base to end-effector once the target pose is reached. Hootsman's controller, however, assumes that gravity effects can be compensated for exactly, which is not necessarily true under varying payload conditions.

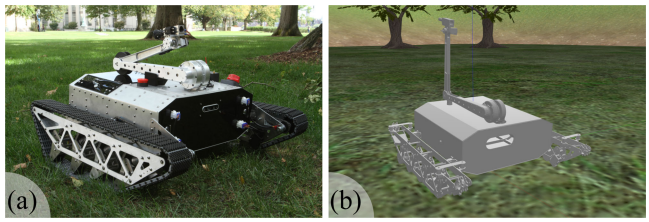

Fig. 1. Picture (a) of the BioInstrumentation Laboratory agricultural robot prototype called Rover II, and screenshot (b) of its Gazebo model simulated in this work.

The desired trajectory of the manipulator can also be preshaped to minimize some relevant cost metrics, such as the norm of reaction forces at the base, the maximum amplitude of base oscillations, or the overall system settling time [4]. For instance, in the special case of redundant flexible-base manipulators, Nenchev proposed to generate trajectories that do not create any reaction at the base [5]. However, such input-shaping approaches are often complemented in practice with vibration-damping feedback, which imposes joint accelerations that are out of phase with the base velocity. George and Book, for instance, successfully demonstrated this approach to control a small rigid manipulator mounted in series with a long, flexible one (also called macro/micromanipulator) [6]. Salehi and Vossoughi later suggested an alternative solution for a suspended mobile manipulator that uses impedance control combined with vibration-damping feedback [7]. To guarantee stability, these solutions assume that oscillations of the base are much faster than the motion of the manipulator, which is not the case for manipulators with low-stiffness bases.

Garofalo recently addressed this limitation using a nonlinear controller based on a momentum-based vibration-damping strategy [8]. The authors were able to guarantee the asymptotic closed-loop stability of the system and showed promising experimental results in comparison to linear alternatives. The controller design, however, assumes that the base link can only move in translation and that there are no viscous friction effects. Both assumptions are not reflective of most vehicle-mounted manipulators. It also includes explicit compensation terms for gravitational, inertial, and Coriolis effects, which are not exactly known in practice. Finally, a significant drawback of any vibration-damping feedback is that it lets the manipulator arbitrarily deviate from its nominal trajectory to achieve the desired

Manuscript received February 19, 2021; accepted June 27, 2021. Date of publication July 16, 2021; date of current version August 3, 2021. This letter was recommended for publication by Associate Editor N. Kottege and P. Pounds upon evaluation of the reviewers' comments. This work was supported by Fonterra Co-operative Group Limited. *(Corresponding author: Marc-André Bégin.)*

The authors are with BioInstrumentation Laboratory, Massachusetts Institute of Technology, Cambridge, MA 02139 USA (e-mail: begin@mit.edu; rpoon@mit.edu; ihunter@mit.edu).

Digital Object Identifier 10.1109/LRA.2021.3097497

damping effect. This limitation complicates collision avoidance. It also makes the control architecture less modular and intuitive than alternatives that treat trajectory generation and tracking as separate tasks.

In a typical mobile robotics setting, the manipulator is likely to handle uncertain loads that require adaptation. Although some real-time trajectory planner in series with joint-space PID control offers a simple solution, the PID control of a manipulator is not guaranteed to be stable (i.e., according to Lyapunov's definition of stability). This is unlike PD controllers, which can be shown to be globally stable and converge to zero error when combined with the appropriate gravity compensation [9]. In the case of fixed-base manipulators, Kelly addressed this issue by deriving a set of sufficient conditions for the local stability of a joint-space PID controller [10]. Loria later showed that delaying the action of the integral term of Kelly's controller results in global stability [11]. However, to the authors' knowledge, there does not exist an equivalent, explicit set of conditions in the case of flexible-base manipulators.

In this letter, Kelly's approach is revisited in the case of a manipulator mounted on a suspended vehicle. Stability conditions for a joint-space PID controller are first derived in Section II. These stability conditions are cast in Section III as a tuning procedure which is applied in Section IV to a simple example in order to help with the understanding of its mechanics. For more complicated models, an open-source Python library is introduced in Section V to streamline the process. The performance of a PID controller tuned with this library is finally assessed in Section VI through simulations of a 3-DOF manipulator mounted on an 8-legged tracked vehicle.

II. Stability Analysis

Consider a manipulator mounted on a suspended vehicle with a total of n degrees of freedom (DOF). The dynamics of the system can be written as

$$\mathrm{H}(\mathbf{x})\ddot{\mathbf{x}} + \mathrm{C}(\mathbf{x}, \dot{\mathbf{x}})\dot{\mathbf{x}} + \mathbf{g}(\mathbf{x}) = \tau, \tag{1}$$

where $\tau \in \mathbb{R}^n$ is the vector combining the passive suspension forces with the ones actively generated by the manipulator's motors, $\mathrm{H} \in \mathbb{R}^{n\times n}$ is the positive definite inertial matrix, $\mathrm{C} \in \mathbb{R}^{n\times n}$ is the centripetal/Coriolis matrix (uniquely defined such that $\dot{\mathrm{H}} - 2\,C$ is skew-symmetric), and $\mathbf{g} \in \mathbb{R}^n$ denotes the vector of gravitational forces. Let the state vector $\mathbf{x} \in \mathbb{R}^n$ be the concatenation of $\mathbf{x}_p \in \mathbb{R}^{n_p}$ and $\mathbf{x}_a \in \mathbb{R}^{n_a}$, which are respectively the n_p variables associated with the passive DOFs of the system, and the n_a variables associated with the DOFs actuated by the motors of the manipulator:

$$\mathbf{x}^{\mathrm{T}} = \begin{bmatrix} \mathbf{x}_p^{\mathrm{T}} & \mathbf{x}_a^{\mathrm{T}} \end{bmatrix}. \tag{2}$$

Similarly, $\mathbf{g}$ can also be decomposed into 2 sub-vectors $\mathbf{g}_p \in \mathbb{R}^{n_p}$ and $\mathbf{g}_a \in \mathbb{R}^{n_a}$ such that

$$\mathbf{g}^{\mathrm{T}}(\mathbf{x}) = \begin{bmatrix} \mathbf{g}_p^{\mathrm{T}}(\mathbf{x}) & \mathbf{g}_a^{\mathrm{T}}(\mathbf{x}) \end{bmatrix}. \tag{3}$$

Let the manipulator's vector of desired angles be denoted as $\mathbf{x}_{a|d} \in \mathbb{R}^{n_a}$. The full state error $\tilde{\mathbf{x}} \in \mathbb{R}^n$ can be accordingly defined as

$$\tilde{\mathbf{x}}^{\mathrm{T}} = \begin{bmatrix} \tilde{\mathbf{x}}_p^{\mathrm{T}} & \tilde{\mathbf{x}}_a^{\mathrm{T}} \end{bmatrix} = \mathbf{x}^{\mathrm{T}} - \underbrace{\begin{bmatrix} \mathbf{x}_p^{*\mathrm{T}} & \mathbf{x}_{a|d}{}^{\mathrm{T}} \end{bmatrix}}_{\mathbf{x}_d}, \tag{4}$$

where $\tilde{\mathbf{x}}_p \in \mathbb{R}^{n_p}$ and $\tilde{\mathbf{x}}_a \in \mathbb{R}^{n_a}$ are respectively the passive and active state errors while $\mathbf{x}_p^* \in \mathbb{R}^{n_p}$ corresponds to the value of the passive states variables at equilibrium once the active DOF settle to their desired position. Because the desired state is static,

$$\dot{\tilde{\mathbf{x}}} = \dot{\mathbf{x}}. \tag{5}$$

Let $\tau_a \in \mathbb{R}^{n_a}$ be the active motor torques of the manipulator determined by a fixed-gain PID controller

$$\tau_a = -\mathrm{K}_P\tilde{\mathbf{x}}_a - \mathrm{K}_D\dot{\mathbf{x}}_a - \mathrm{K}_I\int_0^t \tilde{\mathbf{x}}_a dt, \tag{6}$$

where the symmetric, positive definite matrices $\mathrm{K}_P \in \mathbb{R}^{n_a\times n_a}$, $\mathrm{K}_D \in \mathbb{R}^{n_a\times n_a}$ and $\mathrm{K}_I \in \mathbb{R}^{n_a\times n_a}$ correspond to the PID controller gains which are to be tuned by the procedure. Similarly, let $\tau_p \in \mathbb{R}^{n_p}$, the passive suspension forces acting on the robot chassis, be defined as

$$\tau_p = -\mathrm{K}_s(\mathbf{x}_p)\tilde{\mathbf{x}}_p - \mathrm{B}_s(\mathbf{x}_p)\dot{\mathbf{x}}_p, \tag{7}$$

where $\mathrm{K}_s \in \mathbb{R}^{n_p\times n_p}$ and $\mathrm{B}_s \in \mathbb{R}^{n_p\times n_p}$ are the nonlinear stiffness and damping matrices of the base. To ease off the stability analysis and avoid carrying over the integral from (6), the auxiliary variable $\hat{\mathbf{a}} \in \mathbb{R}^{n_a}$ is defined through the adaptation law

$$\dot{\hat{\mathbf{a}}} = -\tilde{\mathbf{x}}_a - \alpha^{-1}\dot{\mathbf{x}}_a, \tag{8}$$

where α is a positive scalar parameter. Combining (6) to (8), the force vector τ can be concisely written as

$$\tau = \begin{bmatrix} \tau_p \\ \tau_a \end{bmatrix} = -\mathrm{K}\tilde{\mathbf{x}} - \mathrm{B}\dot{\mathbf{x}} + \begin{bmatrix} \mathbf{0} \\ \mathrm{K}_I\hat{\mathbf{a}} \end{bmatrix}, \tag{9}$$

where

$$\mathrm{K} = \begin{bmatrix} \mathrm{K}_s(\mathbf{x}_p) & \mathbf{0} \\ \mathbf{0} & \mathrm{K}_P - \alpha^{-1}\mathrm{K}_I \end{bmatrix},\ \mathrm{K} \in \mathbb{R}^{n\times n}, \tag{10}$$

and

$$\mathrm{B} = \begin{bmatrix} \mathrm{B_s}(\mathbf{x}_p) & \mathbf{0} \\ \mathbf{0} & \mathrm{K}_D \end{bmatrix} > \mathbf{0},\ \mathrm{B} \in \mathbb{R}^{n\times n}. \tag{11}$$

The new auxiliary state variables $\hat{\mathbf{a}}$ can be interpreted as an estimation of the cumulative active state error $\mathbf{a}$ needed to maintain the manipulator in a desired state $\mathbf{x}_{a|d}$. Indeed, from (1) and for $\dot{\mathbf{x}} = \mathbf{0}$, $\ddot{\mathbf{x}} = \mathbf{0}$, and $\dot{\hat{\mathbf{a}}} = \mathbf{0}$,

$$\mathbf{a} = {\mathrm{K}_I}^{-1}\mathbf{g}_a(\mathbf{x}_d). \tag{12}$$

The estimation error $\tilde{\mathbf{a}}$ is then accordingly defined as

$$\tilde{\mathbf{a}} = \hat{\mathbf{a}} - \mathbf{a} = \hat{\mathbf{a}} - {\mathrm{K}_I}^{-1}\mathbf{g}_a(\mathbf{x}_d). \tag{13}$$

To further simplify the stability analysis, let $\mathbf{s} \in \mathbb{R}^n$ be defined as

$$\mathbf{s} = \dot{\tilde{\mathbf{x}}} + \alpha\tilde{\mathbf{x}} = \dot{\mathbf{x}} + \alpha\tilde{\mathbf{x}}. \tag{14}$$

Finally, consider the following candidate Lyapunov function

$$V = \frac{1}{2}\mathbf{s}^{\mathrm{T}}\mathrm{H}\mathbf{s} + \frac{1}{2}\tilde{\mathbf{x}}^{\mathrm{T}}\mathrm{K}\tilde{\mathbf{x}} + P_g + \frac{1}{2}\tilde{\mathbf{a}}^{\mathrm{T}}(\alpha\mathrm{K}_I)\tilde{\mathbf{a}} + \frac{\alpha}{2}\tilde{\mathbf{x}}^{\mathrm{T}}\mathrm{B}\tilde{\mathbf{x}} - \frac{\alpha^2}{2}\tilde{\mathbf{x}}^{\mathrm{T}}\mathrm{H}\tilde{\mathbf{x}} - \tilde{\mathbf{x}}^{\mathrm{T}}\mathbf{g}(\mathbf{x}_d), \tag{15}$$

where $P_g(\mathbf{x})$ is the gravitational potential energy of the system which verifies

$$\frac{\partial P_g(\mathbf{x})}{\partial \mathbf{x}} = \mathbf{g}(\mathbf{x}). \tag{16}$$

The first three terms of V are akin to the total virtual kinetic and potential energy of the system, while the fourth associates a quadratic cost to the estimation error $\tilde{\mathbf{a}}$. The three last terms are carefully introduced to give V and $\dot{V}$ their desired properties.

Consider a bounded region Ω_l defined by $V(\mathbf{x}) < l$. Let $\mathbf{R}$ be the set of all states within Ω_l such that $\dot{V}(\mathbf{x}) = 0$. The largest invariant set in $\mathbf{R}$ only includes the equilibrium at the origin ($\tilde{\mathbf{x}} = \mathbf{0}$, $\dot{\mathbf{x}} = \mathbf{0}$ and $\dot{\hat{\mathbf{a}}} = \mathbf{0}$). Thus, according to the invariant set theorem, the origin has to be a local exponentially stable equilibrium if $V(\mathbf{x})$ is lower bounded and $\dot{V} \leq 0$ for all $\mathbf{x}$ in Ω_l.

Proposition II.1: A sufficient condition for V to be lower bounded is

$$\mathrm{K} > \alpha^2\mathrm{H} + k_g\mathrm{I}_{n\times n}, \tag{17}$$

where

$$k_g \geq \left|\left|\frac{\partial \mathbf{g}(\mathbf{x})}{\partial \mathbf{x}}\right|\right|. \tag{18}$$

Proof: Let V_a be a subset of the terms added to form V such that

$$V_a = \frac{1}{2}\mathbf{s}^{\mathrm{T}}\mathrm{H}\mathbf{s} + \frac{1}{2}\tilde{\mathbf{x}}^{\mathrm{T}}\mathrm{K}\tilde{\mathbf{x}} - \frac{\alpha^2}{2}\tilde{\mathbf{x}}^{\mathrm{T}}\mathrm{H}\tilde{\mathbf{x}}, \tag{19}$$

which can be rewritten in matrix form as

$$V_a = \frac{1}{2}\begin{bmatrix}\dot{\mathbf{x}}\\ \tilde{\mathbf{x}}\end{bmatrix}^{\mathrm{T}} \underbrace{\begin{bmatrix}\mathrm{H} & \alpha\mathrm{H}\\ \alpha\mathrm{H} & \mathrm{K}\end{bmatrix}}_{=\mathrm{Q}} \begin{bmatrix}\dot{\mathbf{x}}\\ \tilde{\mathbf{x}}\end{bmatrix}. \tag{20}$$

For any matrix $\mathrm{D} \in \mathbb{R}^{2n\times 2n}$ that shares the same structure as $\mathrm{Q} \in \mathbb{R}^{2n\times 2n}$, it can be shown [10] that

$$\mathrm{D} = \begin{bmatrix}\mathrm{A} & \mathrm{B}\\ \mathrm{B}^{\mathrm{T}} & \mathrm{C}\end{bmatrix} > 0 \iff \mathrm{A} > 0 \;\; \mathrm{C} - \mathrm{B}^{\mathrm{T}}\mathrm{A}^{-1}\mathrm{B} > 0. \tag{21}$$

Accordingly, Q is positive definite if and only if H is positive definite and if

$$\mathrm{K} > \alpha^2\mathrm{H}. \tag{22}$$

Now, consider a second subset V_b:

$$V_b = P_g(\mathbf{x}) - \tilde{\mathbf{x}}^{\mathrm{T}}\mathbf{g}(\mathbf{x}_d) + \frac{1}{2}\tilde{\mathbf{x}}^{\mathrm{T}}\mathrm{K}\tilde{\mathbf{x}}, \tag{23}$$

such that, using (16),

$$\frac{\partial^2(V_b)}{(\partial \mathbf{x})^2} = \mathrm{K} + \frac{\partial \mathbf{g}(\mathbf{x})}{\partial \mathbf{x}}. \tag{24}$$

Then, V_b is strongly convex and lower bounded if

$$\mathrm{K} > k_g\mathrm{I}_{n\times n}. \tag{25}$$

Conditions (22) and (25) are both fulfilled if (17) is true. Since all other terms in V are positive definite, then V is guaranteed to always be lower bounded. ■

Proposition II.2: A valid upper bound on $\dot{V}$ is

$$\dot{V} \leq -\alpha\tilde{\mathbf{x}}^{\mathrm{T}}\left(\mathrm{K} - k_g\mathrm{I}_{n\times n}\right)\tilde{\mathbf{x}} - \dot{\mathbf{x}}^{\mathrm{T}}\left(\mathrm{B} - \alpha\mathrm{H}\right)\dot{\mathbf{x}} + k_K k_x\left(||\dot{\mathbf{x}}_p|| + \alpha\,||\tilde{\mathbf{x}}_p||\right)||\tilde{\mathbf{x}}_p|| + \alpha k_C\,||\tilde{\mathbf{x}}||\,||\dot{\mathbf{x}}||^2 + \frac{(k_K + \alpha k_B)}{2}||\tilde{\mathbf{x}}_p||^2\,||\dot{\mathbf{x}}_p||, \tag{26}$$

where

$$k_K = n_p\left(\max_{i,j,k,\mathbf{x}}\left|\frac{\partial K_{s|i,j}(\mathbf{x})}{\partial x_k}\right|\right) \forall\; i,\; j,\; k \in \{1, 2, \ldots, m\}, \tag{27}$$

$$k_B = n_p\left(\max_{i,j,k,\mathbf{x}}\left|\frac{\partial B_{s|i,j}(\mathbf{x})}{\partial x_k}\right|\right) \forall\; i,\; j,\; k \in \{1, 2, \ldots, m\}, \tag{28}$$

$$k_x \geq \left|\left|\mathbf{x}_p^*\right|\right| > 0, \tag{29}$$

and

$$k_C \geq \frac{||\mathrm{C}(\mathbf{x}, \dot{\mathbf{x}})\dot{\mathbf{x}}||}{||\dot{\mathbf{x}}||^2}. \tag{30}$$

Proof: Taking the derivative of V and simplifying leads to

$$\dot{V} = -\alpha\tilde{\mathbf{x}}^{\mathrm{T}}\left(\mathrm{K}\tilde{\mathbf{x}} + \mathbf{g}(\mathbf{x}) - \mathbf{g}(\mathbf{x}_d)\right) - \dot{\mathbf{x}}^{\mathrm{T}}(\mathrm{B} - \alpha\mathrm{H})\dot{\mathbf{x}} - \left(\dot{\mathbf{x}}_p + \alpha\tilde{\mathbf{x}}_p\right)^{\mathrm{T}}\left(\mathrm{K}_s(\mathbf{x}_p) - \mathrm{K}_s(\mathbf{x}_p^*)\right)\mathbf{x}_p^* + \alpha\dot{\mathbf{x}}^{\mathrm{T}}\mathrm{C}\tilde{\mathbf{x}} + \frac{1}{2}\tilde{\mathbf{x}}_p^{\mathrm{T}}\left(\dot{\mathrm{K}}_s + \alpha\dot{\mathrm{B}}_s\right)\tilde{\mathbf{x}}_p. \tag{31}$$

Note that when deriving this expression, a useful observation is that at equilibrium, the passive spring forces have to exactly cancel the gravitational forces associated with the passive DOF such that

$$\mathbf{g}_p(\mathbf{x}_d) = -\mathrm{K}_s(\mathbf{x}_p^*)\mathbf{x}_p^*. \tag{32}$$

By the mean value theorem,

$$||\mathbf{g}(\mathbf{x}) - \mathbf{g}(\mathbf{x}_d)|| \leq k_g\,||\tilde{\mathbf{x}}||, \tag{33}$$

such that

$$-\alpha\tilde{\mathbf{x}}^{\mathrm{T}}\left(\mathbf{g}(\mathbf{x}) - \mathbf{g}(\mathbf{x}_d)\right) \leq \alpha k_g\,||\tilde{\mathbf{x}}||^2. \tag{34}$$

Assuming that each element of the stiffness matrix K is bounded, there will always exist a positive constant k_K such that

$$\left(\mathrm{K}_s(\mathbf{x}_p) - \mathrm{K}_s(\mathbf{x}_p^*)\right)\mathbf{x}_p^* \leq k_K\,||\tilde{\mathbf{x}}_p||\,\left|\left|\mathbf{x}_p^*\right|\right|. \tag{35}$$

For instance, (27) provides a valid definition for k_K. Then,

$$-\left(\dot{\mathbf{x}}_p + \alpha\tilde{\mathbf{x}}_p\right)^{\mathrm{T}}\left(\mathrm{K}_s(\mathbf{x}_p) - \mathrm{K}_s(\mathbf{x}_p^*)\right)\mathbf{x}_p^* \leq k_K k_x\left(||\dot{\mathbf{x}}_p|| + \alpha\,||\tilde{\mathbf{x}}_p||\right)||\tilde{\mathbf{x}}_p||. \tag{36}$$

Moreover, from (30),

$$\alpha\dot{\mathbf{x}}^{\mathrm{T}}\mathrm{C}\tilde{\mathbf{x}} \leq \alpha k_C\,||\tilde{\mathbf{x}}||\,||\dot{\mathbf{x}}||^2. \tag{37}$$

Finally, there exists a constant k_B such that

$$\frac{1}{2}\tilde{\mathbf{x}}_p^{\mathrm{T}}\left(\dot{\mathrm{K}}_s+\alpha\dot{\mathrm{B}}_s\right)\tilde{\mathbf{x}}_p \leq \frac{(k_K+\alpha k_B)}{2}\left|\left|\dot{\mathbf{x}}_p\right|\right|\left|\left|\tilde{\mathbf{x}}_p\right|\right|^2. \quad (38)$$

For instance, (28) is a valid definition of k_B. If inequalities (34), (36), (37), and (38) hold, then $\dot{V}$ satisfies (26). ■

Proposition II.3: If Propositions II.1 and II.2 hold, and if

$$\mathrm{B} > \alpha\mathrm{H}, \quad (39)$$

$$\mathrm{K}_s(\mathbf{x}_p) > k\mathrm{I}_{n_p\times n_p}, \quad (40)$$

and

$$\lambda_{\min}\left(\mathrm{B}_s(\mathbf{x}_p)\right) > \frac{\left(k_K k_x\right)^2}{4\alpha\left(\lambda_{\min}\left(\mathrm{K}_s(\mathbf{x}_p)\right)-k\right)}, \quad (41)$$

where

$$k = k_g + k_K k_x > 0, \quad (42)$$

then there exists some region about the origin where $\dot{V} \leq 0$.

Proof: The terms on the first line of (26) are negative definite if (17) and (39) are satisfied. The second line of (26) can be combined with part of the first such that

$$\begin{aligned}&-\alpha\tilde{\mathbf{x}}_p^{\mathrm{T}}\left(\mathrm{K}_s(\mathbf{x}_p)-k_g\mathrm{I}_{n_p\times n_p}\right)\tilde{\mathbf{x}}_p-\dot{\mathbf{x}}_p^{\mathrm{T}}\mathrm{B}_s(\mathbf{x}_p)\dot{\mathbf{x}}_p\\&\quad+k_Kk_x\left(\left|\left|\dot{\mathbf{x}}_p\right|\right|+\alpha\left|\left|\tilde{\mathbf{x}}_p\right|\right|\right)\left|\left|\tilde{\mathbf{x}}_p\right|\right|\\&\leq-\begin{bmatrix}\left|\left|\tilde{\mathbf{x}}_p\right|\right|\\ \left|\left|\dot{\mathbf{x}}_p\right|\right|\end{bmatrix}^{\mathrm{T}}\mathrm{P}\begin{bmatrix}\left|\left|\tilde{\mathbf{x}}_p\right|\right| & \\ & \left|\left|\dot{\mathbf{x}}_p\right|\right|\end{bmatrix},\end{aligned} \quad (43)$$

where

$$\mathrm{P}=\begin{bmatrix}\alpha\left(\lambda_{\min}\left(\mathrm{K}_s(\mathbf{x}_p)\right)-k\right) & -\frac{k_Kk_x}{2}\\ -\frac{k_Kk_x}{2} & \lambda_{\min}\left(\mathrm{B}_s(\mathbf{x}_p)\right)\end{bmatrix}. \quad (44)$$

From (21), $\mathrm{P}\in\mathbb{R}^2$ is positive definite if (40) and (41) are satisfied. Although the two terms on the last line of (26) are positive, they are made of higher order terms. Hence, if Propositions II.1 and II.2 are valid and (39)-(41) are satisfied, then there exists some region about the origin where $\dot{V}\leq 0$. ■

III. Tuning Procedure

For the controller to be stable, V needs to be lower bounded, and $\dot{V}$ needs to be negative semi-definite in some region around the origin, therefore Propositions II.1 and II.3 naturally lead to a tuning procedure. First, explicit conditions on the PID matrices can be obtained by combining (10), (17), and (39) such that

$$\lambda_{\min}(\mathrm{K}_I) > 0, \quad (45)$$

$$\lambda_{\min}(\mathrm{K}_P) > \alpha^2\lambda_{\max}(\mathrm{H}) + \frac{1}{\alpha}\lambda_{\min}(\mathrm{K}_I) + k_g, \quad (46)$$

and

$$\lambda_{\min}(\mathrm{K}_D) > \alpha\lambda_{\max}(\mathrm{H}). \quad (47)$$

Similarly, based on (17), (39), (40), and (41), for some region about the origin, the stiffness and damping matrices associated with the passive base suspension should respect the following inequalities

$$\min_{||\mathbf{x}_p||<k_x}\left(\lambda_{\min}(\mathrm{K}_s(\mathbf{x}_p))\right) > \alpha^2\lambda_{\max}(\mathrm{H}) + k, \quad (48)$$

and

$$\begin{aligned}\min_{||\mathbf{x}_p||<k_x}\left(\lambda_{\min}(\mathrm{B}_s(\mathbf{x}_p))\right) &> \alpha\lambda_{\max}(\mathrm{H})\\ &+\frac{\left(k_Kk_x\right)^2}{4\alpha\left(\lambda_{\min}\left(\mathrm{K}_s(\mathbf{x}_p)\right)-k\right)}.\end{aligned} \quad (49)$$

For any given suspension design (i.e., the expressions for K_s and B_s are known), (48) and (49) specify a valid range for α. More explicitly,

$$\frac{c-\sqrt{(c^2-4b)}}{2} < \alpha < \min\left[a, \frac{c+\sqrt{(c^2-4b)}}{2}\right], \quad (50)$$

where

$$a=\sqrt{\frac{1}{\lambda_{\max}(\mathrm{H})}\left(\min_{||\mathbf{x}_p||<k_x}\left(\lambda_{\min}(\mathrm{K}_s(\mathbf{x}_p))\right)-k\right)} \quad (51)$$

$$b=\frac{\left(k_Kk_x\right)^2}{4\alpha\lambda_{\max}(\mathrm{H})\left(\lambda_{\min}\left(\mathrm{K}_s(\mathbf{x}_p)\right)-k\right)} \quad (52)$$

and

$$c=\frac{\min_{||\mathbf{x}_p||<k_x}\left(\lambda_{\min}(\mathrm{B}_s(\mathbf{x}_p))\right)}{\lambda_{\max}(\mathrm{H})}. \quad (53)$$

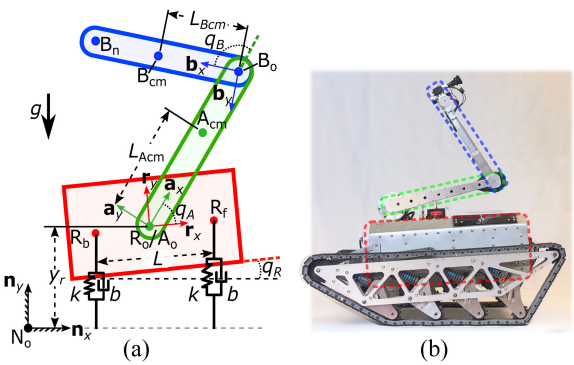

Fig. 2. Side view of RoverII with its manipulator constrained to in-plane motion (a) and its corresponding simple planar model (b) a 2DOF manipulator mounted on a 2DOF passive vehicle suspension.

IV. Case Study: Planar Manipulator

This section demonstrates how the tuning algorithm can be applied directly to the analytical planar model of a mobile manipulator depicted in Fig. 2(a). Albeit simple, this simulated model might capture most of the dynamics of a suspended robot when its manipulator is constrained to in-plane motion (Fig. 2(b)). The suspended frame of the rover is represented by a rigid body R with a center of mass at R_0 and suspension attachment points at R_b and R_f. The robotic manipulator is composed of two segments A and B of length L_A and L_B with the origin of A co-located with R_o. The passive and active state variables $\mathbf{x}_p$

TABLE I
PLANAR MOBILE MANIPULATOR MODEL PARAMETERS

Symbol	Parameter	Value
k	Shock absorber stiffness	124.7 N/m
b	Shock absorber damping constant	56.2 N·s/m
L	Distance from absorber to the other	2.01 m
Selected according to Kelly [10]		
g	Gravitational acceleration	9.81 m/s^2
m_R	R's mass	43.5 kg
m_A	A's mass	9.5 kg
m_B	B's mass	5.0 kg
I_{Rzz}	R's inertia product about $\mathbf{n}_z$	32×10^{-3} kg ·m^2
I_{Azz}	A's inertia product about $\mathbf{n}_z$	4.3×10^{-3} kg·m^2
I_{Bzz}	B's inertia product about $\mathbf{n}_z$	6.1×10^{-3} kg·m^2
L_A	Length of segment A	0.25 m
L_{Acm}	Distance from A's origin to COM	0.20 m
L_B	Length of segment B	0.16 m
L_{Bcm}	Distance from B's origin to COM	0.14 m
Selected according to Section III		
α	Adaptation parameter	0.8
K_I	Integral gain matrix	45.0 $\mathrm{I}_{2\times2}$
K_P	Proportional gain matrix	161.3 $\mathrm{I}_{2\times2}$
K_D	Derivative gain matrix	47.3 $\mathrm{I}_{2\times2}$

amd $\mathbf{x}_a$ of the system are expressed as

$$\mathbf{x}_p = \begin{bmatrix} y_r & q_R \end{bmatrix}^{\mathrm{T}} \text{ and } \mathbf{x}_a = \begin{bmatrix} q_A & q_B \end{bmatrix}^{\mathrm{T}}, \tag{54}$$

where y_r and q_R are R's center of mass height and pitch while q_A and q_B describe the manipulator joint angles with respect to $\mathbf{r}_x$ and $\mathbf{a}_x$ respectively. All model parameters are defined in Table I and were selected such that the manipulator has the same dynamics as the fixed-base manipulator introduced in Kelly's original letter [10]. Explicit expressions for each term of the model (1) applied to this example are available in Appendix I. For this simple 2D case, algebraic expressions for the constants used in the tuning procedure (k_g, k_x, k_K and k_B) can easily be derived and are provided in Appendix II. For more complex models such as the one presented in Section VI, these can also be approximated numerically. Based on the suspension parameters, (50) implies

$$0.016 < \alpha < 1.664. \tag{55}$$

For instance, α can be set to 0.8. The values for K_I, K_P and K_D set in Table I also verify (45 - 47).

The resulting PID controller is thus guaranteed to be stable about some region around the origin. To gain intuition on the size of this stability region, it is useful to evaluate and visualize some upper bound on V and $\dot{V}$. These bounds can be derived by hand in this simple 2D case or can be numerically approximated for more complex models. First, from (15),

$$\begin{aligned} V \leq\ & \frac{1}{2}\lambda_{\max}(\mathrm{H})\,||\mathbf{s}||^2 + \frac{1}{2}\left(\lambda_{\max}(\mathrm{K})\right. \\ & \left. + \alpha\lambda_{\max}(\mathrm{B}) - \alpha^2\lambda_{\min}(\mathrm{H})\right)||\tilde{\mathbf{x}}||^2 \\ & + P_g + \frac{1}{2}\tilde{\mathbf{a}}^{\mathrm{T}}(\alpha\mathrm{K}_I)\tilde{\mathbf{a}} + \max(||\mathbf{g}(\mathbf{x}_d)||)\,||\tilde{\mathbf{x}}||\,. \end{aligned} \tag{56}$$

Noting that

$$P_g \leq m_{\mathrm{tot}} g\,|y_r| + c \leq m_{\mathrm{tot}} g\,||\tilde{\mathbf{x}}_p|| + c, \tag{57}$$

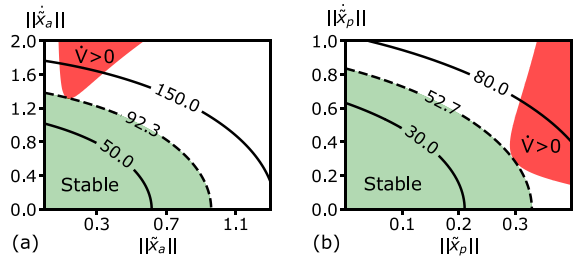

Fig. 3. Contour plots of ξ for the PID controller of a planar flexible-base manipulator.

where m_{tot} is the total mass of the system and c is some arbitrary constant, then

$$V \leq \xi + \frac{1}{2}\tilde{\mathbf{a}}^{\mathrm{T}}(\alpha\mathrm{K}_I)\tilde{\mathbf{a}} + c, \tag{58}$$

where

$$\begin{aligned} \xi = & \frac{1}{2}\lambda_{\max}(\mathrm{H})\,||\mathbf{s}||^2 + \frac{1}{2}\left(\lambda_{\max}(\mathrm{K})\right. \\ & \left. + \alpha\lambda_{\max}(\mathrm{B}) - \alpha^2\lambda_{\min}(\mathrm{H})\right)||\tilde{\mathbf{x}}||^2 \\ & + m_{\mathrm{tot}} g\,||\tilde{\mathbf{x}}_p|| + \max(||\mathbf{g}(\mathbf{x}_d)||)\,||\tilde{\mathbf{x}}||\,. \end{aligned} \tag{59}$$

Moreover, from inequality (26),

$$\begin{aligned} \dot{V} \leq\ & -\alpha\left(\lambda_{\min}(\mathrm{K}_s(\mathbf{x}_p)) - k\right)||\tilde{\mathbf{x}}_p||^2 \\ & - \lambda_{\min}(\mathrm{B}_s(\mathbf{x}_p))\,||\dot{\mathbf{x}}_p||^2 \\ & - \alpha(\lambda_{\min}(\mathrm{K}_P - \alpha^{-1}\mathrm{K}_I) - k_g)\,||\tilde{\mathbf{x}}_a||^2 \\ & - \lambda_{\min}(\mathrm{K}_D)\,||\dot{\mathbf{x}}_a||^2 \\ & + \alpha\lambda_{\max}(\mathrm{H})\,||\dot{\mathbf{x}}||^2 + k_K k_x\left(||\dot{\mathbf{x}}_p|| + \alpha\,||\tilde{\mathbf{x}}_p||\right)||\tilde{\mathbf{x}}_p|| \\ & + \alpha k_C\,||\tilde{\mathbf{x}}||\,||\dot{\mathbf{x}}||^2 + \frac{1}{2}\left(\mathrm{k}_K\right. \\ & \left. + \alpha\mathrm{k}_B\right)||\tilde{\mathbf{x}}_p||^2\,||\dot{\mathbf{x}}_p||\,. \end{aligned} \tag{60}$$

One may also define ℓ as the right-hand side of inequality (60) such that

$$\dot{V} \leq \ell. \tag{61}$$

Consider the case where the manipulator angular position and speed errors are initially zero ($\tilde{\mathbf{x}}_a = 0$ and $\dot{\mathbf{x}}_a = 0$) as shown in Fig. 3(a). The guaranteed region of attraction (green) is then delimited by the isometric line with the largest value of ξ that does not intersect the region where $\ell > 0$ (red). Similarly, Fig. 3(b) shows the guaranteed region of attraction for the case where the passive degrees of freedom of the system are initially at rest ($\tilde{\mathbf{x}}_p = 0$ and $\dot{\mathbf{x}}_p = 0$).

As the control gains found using the tuning procedure proposed in this letter are not unique, these plots are useful to visualise the impact of changing some of the PID control parameters on the stability of the controller. Moreover, the upper bounds on $||\tilde{\mathbf{x}}_p||$, $||\tilde{\mathbf{x}}_a||$, $||\dot{\mathbf{x}}_p||$, and $||\dot{\mathbf{x}}_a||$ obtained when approximating the stability regions using rectangular fits could also be used for instance to constrain the output of a trajectory planner feeding the desired manipulator trajectory to the PID controller.

V. AUTOTUNER LIBRARY

To generate systematically a stable PID controller and its corresponding stability region plots for a wide range of models for serial manipulators mounted on a passively suspended base, the proposed tuning algorithm was implemented as an open-source Python library [12]. Based on the work of Hauser [13], the script numerically evaluates $\mathrm{H}(\mathbf{x})$, $\mathbf{g}(\mathbf{x})$, and $\mathrm{C}(\mathbf{x}, \dot{\mathbf{x}})$ as callback functions. These are automatically generated from the known dynamics of the base and manipulator described using the popular Universal Robot Description Format (URDF). The stiffness $\mathrm{K}_s(\mathbf{x})$ and damping $\mathrm{B}_s(\mathbf{x})$ matrices of the base passive suspension are fed to the algorithm using user-defined callback functions.

The tuning procedure detailed in Section III depends on the few constant parameters k_g, k_K, k_B, k_x, and k_c respectively defined by (18), (27), (28), (29), and (37). The minimum and maximum eigenvalues of the mass, stiffness, and damping matrices are also required. In the provided library, a Nelder-Mead downhill simplex minimization algorithm operating over the whole state space is employed to solve numerically for each of these constants.

Once complete, the algorithm outputs a valid range for α and lower bounds on $\lambda_{\min}(\mathrm{K}_P)$ and $\lambda_{\min}(\mathrm{K}_D)$, which are graphically represented for varying values of α (over the valid range) and $\lambda_{\min}(\mathrm{K}_I)$. Once the user selects valid PID parameters, the corresponding stability regions can easily be generated using a provided utility function.

VI. CASE STUDY: 8-LEGGED ROVER

This section will now demonstrate how the autotuner library can be directly applied to a simulated 3DOF manipulator mounted on an 8-legged rover. The dimensions and other physical parameters of this model were selected to match those of a real-life suspended tracked robot developed in the MIT BioInstrumentation Laboratory (Fig. 1(a)). To limit the scope of the analysis, it is assumed that the robot tracks are not moving during manipulation. Under this assumption, the robot's center of mass does not undergo significant motion in the horizontal plane, therefore its state can be captured by 3 degrees of freedom: the height z of the chassis center of mass, the chassis roll ϕ, and pitch θ. The three active joints the manipulator are respectively described as q_1, q_2, and q_3.

The URDF file and the callback functions defining the dynamic model of this mobile manipulator and its suspension can be found in the examples sub-folder of the library [12]. The bounds determined by running the tuning algorithm on this model are represented in Fig. 4. Given these bounds, let for instance

$$\alpha = 0.5,\ \mathrm{K}_I = 25.0\,\mathrm{I},\ \mathrm{K}_P = 70.4\,\mathrm{I},\ \mathrm{K}_D = 13.5\,\mathrm{I}, \quad (62)$$

where $\mathrm{I} \in \mathbb{R}^{3\times3}$. The stability regions associated with this PID controller are presented in Fig. 5.

To validate the performance of the resulting PID controller, the flexible-base manipulator described above is simulated using the ODE physics engine within Gazebo's environment. A rendering of the Gazebo model is included in Fig. 1(b). In these simulations, a model-predictive motion planner feeds the desired joint angles to the PID controller. The planner employs Levenberg-Marquardt's least squares optimizer to solve for the desired joint angle trajectories that minimize the functional J defined as

$$J = \int_0^{t_{\mathrm{end}}} \left(\left(\mathbf{x} - \mathbf{x}^{\mathrm{ref}}\right)^{\mathrm{T}} \mathrm{W} \left(\mathbf{x} - \mathbf{x}^{\mathrm{ref}}\right) + \ddot{\mathbf{x}}_a^{\mathrm{T}} \mathrm{R} \ddot{\mathbf{x}}_a \right) dt, \quad (63)$$

where $\mathbf{x}^{\mathrm{ref}}$ is the target final state and where the weighting matrices $\mathrm{W} \in \mathbb{R}^{n\times n}$ and $\mathrm{R} \in \mathbb{R}^{n_a \times n_a}$ can be tweaked to generate more or less aggressive trajectories. For any given trajectory candidate assessed by the optimizer, J is evaluated numerically by simulating a simplified model of the manipulator, which assumes perfect tracking of desired trajectories by the PID joint controller. The resulting manipulator joint trajectories thus reduce the time required by the overall system to reach equilibrium, including the passive degrees of freedom of the suspension. In this case, W and R were set to identity matrices factored by 0.01 and 3, respectively. The control time horizon t_{end} was set to 0.2 seconds to limit the required computation time.

The state trajectories resulting from a series of Gazebo simulations where the manipulator is moved to 36 different orientations are shown in Fig. 6 with their corresponding average RMS tracking errors in Table II. In scenario (a), the PID gains

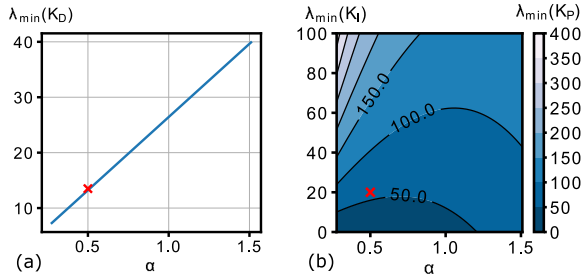

Fig. 4. In (a), the region above the line represents valid values for $\lambda_{\min}(\mathrm{K}_D)$. In (b), contour lines show the lower bound on $\lambda_{\min}(\mathrm{K}_P)$. Red marks designate the selected settings.

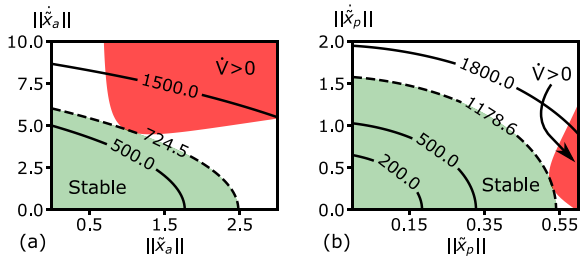

Fig. 5. Contour plots of ξ for the PID controller of a 3DOF flexible-base manipulator.

TABLE II
AVERAGE PERFORMANCE METRICS OF TWO PID CONTROLLERS OVER ALL 3 ACTIVE JOINTS FOR 36 DESIRED TRAJECTORIES

	RMS tracking error (rad)	Settling time (s)	Overshoot (%)
Not tuned	0.305	2.391	32.799
Tuned	0.184	2.047	0.004

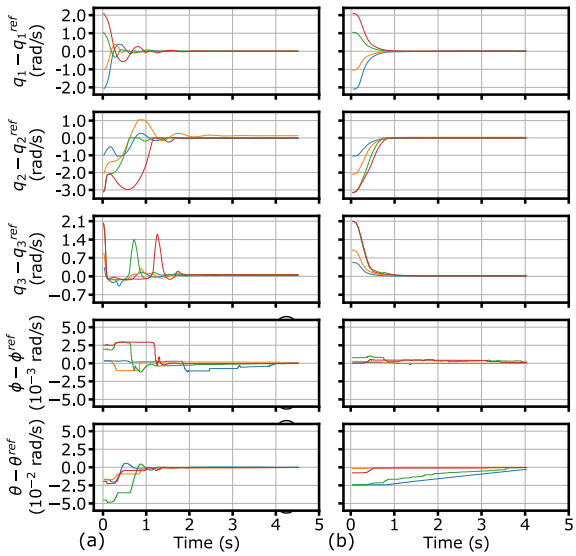

Fig. 6. Angular error trajectories of active states (q_1, q_2, q_3) and passive states (ϕ roll and θ pitch) when the manipulator moves from rest and $\hat{\mathbf{a}}|_{t=0} = \mathbf{0}$. In (a), the PID gains are not tuned while in (b), the PID gains are tuned. Note the height z of the robot is not shown for concision.

are intentionally tuned off such that they do not respect the conditions of the tuning procedure while scenario (b) uses the parameters set in (62). Specifically, for (a), the derivative gain was set to 7.4 % of its proper value. As shown in Table II, proper PID tuning reduces the average joint overshoot and average joint settling time by more than 0.3 s and 30 %, respectively. The average RMS tracking error was also reduced by more than 0.1 rd when the tuning procedure was applied.

VII. Conclusion

This letter addressed the definition of a tuning procedure to obtain stable PID gains operating in the joint space of a flexible-base manipulator. The intuition behind the mechanics of the algorithm was provided through a detailed implementation of the tuning procedure for a simple planar model of a flexible-base manipulator. In addition, the open-source library provided along with this work streamlines the process of applying the tuning procedure to a wide array of flexible-base manipulators. Finally, a practical example of applying this code to a simulated 3D model of a 3DOF manipulator mounted on a 3DOF flexible base demonstrates the usefulness of the approach when the PID controller is used in series with a model-predictive trajectory planner, which reduces the settling time of the passive suspension.

Compared to other solutions suggested in the literature for flexible-base manipulators, the proposed approach is intuitive to implement and modular since the PID controller can be combined with any user-defined trajectory planner. Its stability also does not require a separation of bandwidths between the dynamics of the manipulator and the flexible base. Moreover, unlike other methods which include direct feedback terms on base vibrations, the proposed approach does not allow the manipulator to arbitrarily deviate from its reference trajectory to dampen the base.

Future work on this tuning procedure will include the generation of metrics quantifying the robustness of the controller with respect to parametric uncertainties and external disturbances such as vibrations and vehicle acceleration in the case of mobile-base manipulators.

Appendix I: Dynamics of the 2D Manipulator

This appendix includes the algebraic expressions describing the 2D manipulator dynamics (Section IV).

Constant Parameters

$$a_1 = k, \quad a_2 = b, \quad a_3 = I_{Bzz}, \quad a_4 = m_A g + m_B g + m_R g$$
$$a_5 = m_A + m_B + m_R, \quad a_6 = m_B L_{Bcm}, \quad a_7 = m_A L_{Acm}$$
$$a_8 = m_A g L_{Acm}, \quad a_9 = m_B g, \quad a_{10} = m_B L_A L_{Bcm}$$
$$a_{11} = I_{Azz} + I_{Bzz} + m_A L_{Acm}^2, \quad a_{12} = L_A^2 + L_{Bcm}^2$$
$$a_{13} = L_A L_{Bcm}, \quad a_{14} = I_{Azz} + a_3 + I_{Rzz} + m_A L_{Acm}^2$$
$$a_{15} = m_B g L_{Bcm}, \quad a_{16} = a_3 + m_B L_{Bcm}^2, \quad a_{17} = m_B L_A$$
$$a_{18} = a_1 L_{\text{offset}}, \quad a_{19} = L_A a_9, \quad a_{20} = a_2\, L$$
$$a_{21} = a_1\, L, \quad a_{22} = L_{Bcm} a_9, \quad a_{23} = m_B a_{12}$$
$$a_{24} = L_{Bcm} a_6, \quad a_{25} = a_1\, L^2, \quad a_{26} = a_2\, L^2$$

Matrix $\mathrm{H}(\mathbf{x})$

$$H_{11} = a_5, \quad H_{13} = H_{12}$$
$$H_{12} = (a_7 + a_{17})\cos(q_A + q_R) + a_6 \cos(q_A + q_B + q_R)$$
$$H_{14} = a_6 \cos(q_A + q_B + q_R)$$
$$H_{21} = H_{12}, \quad H_{22} = a_{14} + a_{23} + 2a_{10}\cos(q_B)$$
$$H_{23} = a_{11} + a_{23} + 2a_{10}\cos(q_B)$$
$$H_{24} = a_3 + a_{24} + a_{10}\cos(q_B)$$
$$H_{31} = H_{13} = H_{12}, \quad H_{32} = H_{23}$$
$$H_{33} = H_{32} = H_{23}, \quad H_{34} = H_{24}$$
$$H_{41} = H_{14}, \quad H_{42} = H_{24}, \quad H_{43} = H_{34}, \quad H_{44} = a_{16}$$

Vector $\mathbf{g}(\mathbf{x})$

$$g_1 = 0,\ g_3 = g_2, \quad g_4 = a_{15}\cos(q_A + q_B + q_R),$$
$$g_2 = (a_8 + a_{19})\cos(q_A + q_R) + a_{22}\cos(q_A + q_B + q_R).$$

Matrix $\mathrm{C}(\mathbf{x}, \dot{\mathbf{x}})$

$$C_{11} = C_{21} = C_{31} = C_{41} = 0, \quad C_{13} = C_{12}$$
$$C_{12} = -a_6 \sin(q_A + q_B + q_R)(\dot{q}_A + \dot{q}_B + \dot{q}_R) - (a_7 + a_{17})\sin(q_A + q_R)(\dot{q}_A + \dot{q}_R)$$
$$C_{14} = -a_6 \sin(q_A + q_B + q_R)(\dot{q}_A + \dot{q}_B + \dot{q}_R)$$

$$C_{22} = -a_{10}\sin(q_B)\dot{q}_B, \quad C_{23} = C_{22}$$
$$C_{24} = -a_{10}\sin(q_B)(\dot{q}_A + \dot{q}_B + \dot{q}_R)$$
$$C_{32} = C_{22}, \quad C_{33} = C_{22}, \quad C_{34} = C_{24}$$
$$C_{42} = a_{10}\sin(q_B)(\dot{q}_A + \dot{q}_R), \quad C_{43} = C_{42}, \quad C_{44} = 0$$

Matrix $\mathbf{K}_s(\mathbf{x})$ Note that the equivalent rotational spring torque τ_{eq} of the rover body is given by

$$\tau_{\text{eq}} = \frac{a_{25}}{2}\sin(q_R)\cos(q_R). \tag{64}$$

Noting that the model is only valid for $-\frac{\pi}{2} \leq q_r \leq \frac{\pi}{2}$, it can be approximated as

$$\hat{\tau}_{\text{eq}}(q_r) = \frac{a_{25}}{2}(1 - 0.6369q_r^2 + 0.0939q_r^4)q_r, \tag{65}$$

such that

$$K_{11} = 2a_1, \qquad K_{22} = \frac{a_{25}}{2}(1 - 0.6369q_r^2 + 0.0939q_r^4),$$
$$K_{12} = K_{21} = 0.$$

Matrix $\mathbf{B_s}(\mathbf{x})$

$$B_{11} = 2a_2,\ B_{22} = \frac{a_{26}}{2}\cos(q_R)^2,\ B_{12} = B_{21} = 0.$$

Appendix II: Tuning Algorithm Parameters of the 2D Manipulator

This section includes explicit expressions for k_g, k_C, k_x, k_K and k_B for the 2D manipulator (Section IV). From (18),

$$k_g = 4(a_8 + a_{19} + a_{22}). \tag{66}$$

Moreover,

$$\mathrm{C}(\mathbf{x}, \dot{\mathbf{x}})\dot{\mathbf{x}} = \begin{bmatrix} q_R \\ q_A \\ q_B \end{bmatrix}^{\mathrm{T}} \underbrace{\begin{bmatrix} m_1(\mathbf{x}) & m_1(\mathbf{x}) & m_2(\mathbf{x}) \\ m_1(\mathbf{x}) & m_1(\mathbf{x}) & m_2(\mathbf{x}) \\ m_2(\mathbf{x}) & m_2(\mathbf{x}) & m_2(\mathbf{x}) \end{bmatrix}}_{\mathrm{M}} \begin{bmatrix} q_R \\ q_A \\ q_B \end{bmatrix}, \tag{67}$$

where, using the constant vector $\mathbf{a}$ defined in Appendix I,

$$\begin{aligned} m_1(\mathbf{x}) &= a_{10}\sin(q_B) - (a_7 + a_{17})\sin(q_A + q_R) \\ &\quad - a_6\sin(q_A + q_B + q_R), m_2(\mathbf{x}) \\ &= -2a_{10}\sin(q_B) - a_6\sin(q_A + q_B + q_R). \end{aligned} \tag{68}$$

Dropping the arguments, the largest eigenvalue of M can be written as

$$\lambda_{\max}(\mathrm{M}) = m_1 + \frac{m_2}{2} + \frac{1}{2}\sqrt{4\,m_1^2 - 4m_1m_2 + 9\,m_2^2}, \tag{69}$$

which is maximized when both m_1 and m_2 are. A valid choice for k_C is therefore

$$k_C = m_1^* + \frac{m_2^*}{2} + \frac{1}{2}\sqrt{4\,(m_1^*)^2 - 4\,m_1^*\,m_2^* + 9\,(m_2^*)^2}, \tag{70}$$

where

$$m_1^* = a_{10} + a_7 + a_{17} + a_6, m_2^* \quad = 2a_{10} + a_6. \tag{71}$$

Because the pre-compression of the suspension springs exactly cancels off the total weight $(m_A + m_B + m_R)$ of the system and given the geometry of the problem, one should note that if there are no external disturbances, then y_r will always be 0 at equilibrium such that $||\mathbf{x}_p^*|| = |q_R^*|$. Moreover, at equilibrium

$$\begin{aligned} \mathbf{g}_p(\mathbf{x}_d) &= -\mathrm{K}_s(\mathbf{x}_d)\mathbf{x}_p^* \Leftrightarrow g_2(\mathbf{x}_d) \\ &= -K_{22}(q_r^*)q_r^* = -\frac{a_{25}}{2}\sin(q_r^*)\cos(q_r^*) \Leftrightarrow q_r^* \\ &= \frac{1}{2}\arcsin\left(-\frac{4g_2(\mathbf{x}_d)}{a_{25}}\right), \end{aligned} \tag{72}$$

such that

$$\begin{aligned} |q_r^*| &\leq \frac{1}{2}\arcsin\left(\frac{4\max(|g_2(\mathbf{x}_d)|)}{a_{25}}\right) \\ &\Leftrightarrow |q_r^*| \leq \frac{1}{2}\arcsin\left(\frac{4(a_8 + a_{19} + a_{22})}{a_{25}}\right) = k_x. \end{aligned} \tag{73}$$

Directly using (27) and (28),

$$k_K \approx (0.4362)a_{25},\ k_B = \frac{a_{26}}{2}. \tag{74}$$

References

[1] N. Hootsmans and S. Dubowsky, "Large motion control of mobile manipulators including vehicle suspension characteristics,"in *Proc. IEEE Int. Conf. Robot. Automat. Sacramento*, CA, USA: IEEE Comput. Soc. Press, 1991, pp. 2336–2341.

[2] N. Hootsmans, S. Dubowsky, and P. Mo, "The experimental performance of a mobile manipulator control algorithm," in *Proc. IEEE Int. Conf. Robot. Automat.*, Nice, France: IEEE Comput. Soc. Press, 1992, pp. 1948–1954.

[3] M. Torres, S. Dubowsky, and A. Pisoni, "Vibration control of deployment structures' long-reach space manipulators: The P-PED Method," in *Proc. IEEE Int. Conf. Robot. Automat.*, Minneapolis, MN, USA: IEEE, vol. 3, pp. 2498–2504, 1996.

[4] N. C. Singer and W. P. Seering, "Preshaping command inputs to reduce system vibration," *ASME J. Dyn. Syst., Meas., Control*, vol. 112, pp. 76–82, 1990.

[5] D. Nenchev, K. Yoshida, P. Vichitkulsawat, and M. Uchiyama, "Reaction null-space control of flexible structure mounted manipulator systems," *IEEE Trans. Robot. Automat.*, vol. 15, no. 6, pp. 1011–1023, Dec. 1999.

[6] L. George and W. Book, "Inertial vibration damping control of a flexible base manipulator," *IEEE/ASME Trans. Mechatronics*, vol. 8, no. 2, pp. 268–271, Jun. 2003.

[7] M. Salehi and G. R. Vossoughi, "High-precision impedance control method for flexible base moving manipulators," *Adv. Robot.*, vol. 23, no. 1-2, pp. 65–87, Jan. 2009.

[8] G. Garofalo, F. Beck, J. Klodmann, and C. Ott, "On the control of translationally flexible base manipulators," in *Proc. Eur. Control Conf.*. Saint Petersburg, Russia: IEEE, 2020, pp. 867–874.

[9] M. Takegaki and S. Arimoto, "A new feedback method for dynamic control of manipulators," *J. Dyn. Syst., Meas., Control*, vol. 103, no. 2, pp. 119–125, Jun. 1981.

[10] R. Kelly, "A tuning procedure for stable PID control of robot manipulators," *Robotica*, vol. 13, no. 2, pp. 141–148, Mar. 1995.

[11] A. Loria, E. Lefeber, and H. Nijmeijer, "Global asymptotic stability of robot manipulators with linear PID and PI2D control," *Stability and Control: Theory and Applications*, vol. 3, no. 2, pp. 138–149, 2000.

[12] R. Poon and M.-A. Bégin, "Flexible-Base manipulator control Autotuner," 2021. [Online]. Available: https://github.com/ryanp543/autotuner.git

[13] K. Hauser, "Robust contact generation for robot simulation with unstructured meshes," in *Proc. Int. Symp. Robot. Res.*, 2016, pp. 357–373.